Hierarchical Action and Inhibition of Plant Dicer-Like Proteins in Antiviral Defense

Angélique Deleris[1], Javier Gallego-Bartolomé[1], Jinsong Bao[2], Kristin D. Kasschau[2], James C. Carrington[2], Olivier Voinnet[1*]

1. Institut de Biologie Moléculaire des Plantes, CNRS Unité Propre de Recherche (UPR) 2357, 12, rue du Général Zimmer, 67084 Strasbourg Cedex, France.

2. Center for Genome Research and Biocomputing, Oregon State University, Corvallis, OR 97331, USA.

*To whom correspondence should be addressed. E-mail: olivier.voinnet@ibmp-ulp.u-strasbg.fr

This article has a correction.
Please see: Erratum for the Research Article “Hierarchical action and inhibition of plant Dicer-like proteins in antiviral defense” by A. Deleris, J. Gallego-Bartolome, J. Bao, K. D. Kasschau, J. C. Carrington, O. Voinnet - 22 January 2016

Abstract

The mechanisms underlying induction and suppression of RNA silencing in the ongoing plant-virus arms race are poorly understood. We show here that virus-derived small RNAs produced by *Arabidopsis* Dicer-like 4 (DCL4) program an effector complex conferring antiviral immunity. Inhibition of DCL4 by a viral-encoded suppressor revealed the subordinate antiviral activity of DCL2. Accordingly, inactivating both DCL2 and DCL4 was necessary and sufficient to restore systemic infection of a suppressor-deficient virus. The effects of DCL2 were overcome by increasing viral dosage in inoculated leaves, but this could not surmount additional, non–cell autonomous effects of DCL4 specifically preventing viral unloading from the vasculature. These findings define a molecular framework for studying antiviral silencing and defense in plants.

In RNA silencing, ribonuclease (RNase) III–like enzymes in the Dicer family produce short interfering (si)RNA and micro (mi)RNA from RNA with double-stranded (ds) features (*1*). These molecules guide RNA-induced silencing complexes (RISCs) to suppress gene expression at the transcriptional, RNA-stability, and translational levels (*2*). *Arabidopsis thaliana* has four specialized Dicer-like (DCL) proteins. DCL1 processes fold-back precursors to release miRNAs (*3*). DCL3 produces 24–nucleotide (nt)–long, DNA repeat–associated siRNAs guiding heterochromatin formation (*4*). DCL4 generates 21-nt-long siRNAs that mediate posttranscriptional silencing of some endogenous genes [trans-acting (ta)–siRNAs; (*5*, *6*)] and of transgenes mediating RNA interference (*7*). DCL2 synthesizes stress-related natural-antisense-transcript (nat)–siRNAs (*8*), siRNAs derived from at least one virus (*4*), and, in *dcl4* mutant plants, it alternately processed ~22-nt siRNAs from ta-siRNA precursors (*5*, *6*).

The observations that virus-derived siRNAs accumulate in plant and insect infected tissues and that many viruses encode suppressor proteins targeting DCL, RISC, or small RNA activities strongly suggest that RNA silencing has antiviral roles (*9*–*11*). In plants, one or more of the six RNA-dependent RNA-polymerase (RDR) paralogs, including *Arabidopsis* RDR6 and RDR1, may strengthen primary silencing responses by producing dsRNA from viral templates (*12*) and by amplifying mobile silencing signals conditioning antiviral immunity in non-infected tissues (*7*, *13*). Nevertheless, the genetic bases of silencing induction and suppression by plant viruses remain unclear. Even the existence of an antiviral RISC ("slicer") is arguable because DCL-mediated processing of virus-derived dsRNA could be, in principle, sufficient to dampen infections. It remains also uncertain how, when, and where antiviral silencing and its suppression impact susceptibility and defense in whole plants. This study addresses these issues using *Arabidopsis* silencing mutants and three distinct RNA viruses.

DCL4- and DCL2-dependent siRNAs recruit an antiviral RISC.

Arabidopsis plants were inoculated with modified *Tobacco rattle virus* (TRV-PDS) (Fig. 1A) containing a fragment of the *Arabidopsis* phytoene desaturase (*PDS*) gene in place of the RNA2-encoded 2b and 2c sequences. Like TRV-infected tissues (Fig. 1B), TRV-PDS–infected tissues are free of disease symptoms, because of a strong silencing response that dramatically reduces viral titers (*14*), and exhibit extensive photobleaching due to virus-induced gene silencing (VIGS) of *PDS* (Fig. 1C) (*7*).

TRV-PDS–specific siRNAs accumulated as discrete 21-nt and 24-nt species in wild-type (WT) *Arabidopsis* (Fig. 1D), a pattern unchanged in *rdr1, rdr2, rdr6* [supporting online material (SOM), fig. S1], and *dcl2* mutants (Fig. 1D). However, the 24-nt and 21-nt siRNAs were undetectable in *dcl3* and *dcl4* mutants, respectively. Loss of 21-nt siRNAs coincided with appearance of 22-nt siRNAs in *dcl4* mutants (Fig. 1D). Identical siRNA patterns were detected with an RNA2(TRV)-specific probe,

whereas probes specific for cellular *PDS* sequences absent in TRV-PDS yielded no signal, which indicated that all siRNA species detected were of viral origin (fig. S1). Viral RNA accumulation was not altered in any of the single *dcl* or *rdr* mutants, nor was the extent and/or consistency of VIGS compared with WT-infected plants (Fig. 1, D and F to I) (fig. S1), which suggested redundancy among those factors in mediating antiviral silencing.

dcl combination mutants were then infected. Like *dcl3, dcl2-dcl3* double mutants accumulated only 21-nt siRNAs and had unaltered TRV-PDS levels and VIGS phenotype (Fig. 1, E and J). Similar infection and VIGS phenotypes were detected in *dcl3-dcl4* double mutants, although they accumulated exclusively 22-nt siRNAs (Fig. 1, E and K). By contrast, VIGS was abolished in *dcl2-dcl4* plants accumulating only 24-nt siRNAs. This coincided with higher virus RNA levels and stronger disease symptoms (Fig. 1, E and L), also observed in *dcl2-dcl3-dcl4* triple mutants, in which low-abundance, DCL1-dependent siRNAs were detected (Fig. 1M; fig. S1).

Although the DCL3-dependent, 24-nt siRNA accumulated to the same high levels as 21-nt and 22-nt siRNAs (Fig. 1, D and E), it was neither necessary (Fig. 1D) nor sufficient (Fig. 1E) to mediate VIGS and defense against TRV. Thus, the DCL3-dependent dicing reaction alone could not limit virus infection. The additional requirement for an siRNA-loaded RISC was evidenced by the fact that loss of slicer activity (i.e., *PDS* VIGS), appearance of disease symptoms, and high virus accumulation were inherently correlated in *dcl2-dcl4*. We conclude that the respective 21-nt and 22-nt siRNA products of DCL4 and DCL2 (Fig. 1, D and E) guide an antiviral RISC to promote defense against TRV. DCL2 likely acts as a DCL4 substitute because its activity was contingent on DCL4 loss of function.

TCV-encoded P38 suppresses DCL4.

To assess the generality of these findings and the significance of a DCL4 substitute, we analyzed infection by *Turnip crinkle virus* (TCV, Fig. 2A). Unlike TRV, TCV causes disease symptoms in WT *Arabidopsis* (fig. S2) and encodes a strong silencing suppressor, the P38 capsid protein (*15*). In WT *Arabidopsis*, TCV-derived siRNAs accumulated as a single, 22-nt species. This profile was not changed in *dcl3, dcl4*, or *dcl3-dcl4* mutants (Fig. 2A) and not in *rdr1, rdr2*, or *rdr6* backgrounds (fig. S2). By contrast, 22-nt siRNA levels were strongly reduced in *dcl2* mutants, as has been reported (*4*), and in *dcl2-dcl3* and *dcl2-dcl4* double mutants (Fig. 2A). A time-course analysis revealed that all single, double, and triple mutants with *dcl2* mutations accumulated statistically higher TCV RNA levels than did WT plants or mutants without *dcl2* (Fig. 2B). However, these effects were modest (up to twofold), as also revealed by P38 immunoblots and symptom evaluation (Fig. 2A and fig. S2), and were disproportionate compared with the near-loss of 22-nt siRNAs in *dcl2* and its derivatives.

Previous studies suggested that DCL2 functions redundantly with at least one other DCL (*4*), and we envisaged that P38 effectively masked the effects of this second TCV-antagonizing activity. To test this hypothesis, we analyzed P38-expressing *Arabidopsis* that also expressed a second inverted-repeat (IR) transgene producing siRNAs against the chalcone synthase (*CHS*) mRNA (Fig. 2C). Transgenic P38 restored *CHS* accumulation, significantly reduced 21-nt *CHS* siRNA levels, and triggered accumulation of less abundant, 22-nt siRNAs (Fig. 2C, left panel). This resembled the TRV-PDS siRNA patterns in DCL4-deficient mutants (Fig. 1, D and E), which suggested that P38 suppresses DCL4. Accordingly, endogenous DCL4-dependent ta-siRNAs were specifically lost in P38 plants (Fig. 2C, left). TCV infection recapitulated all these DCL4-suppressing effects (Fig. 2C, right). These data suggested that both DCL4 and DCL2 mediate TCV silencing, with DCL2 providing redundant siRNA-processing functions when DCL4 is suppressed by P38.

DCL4 and DCL2 redundantly silence P38-deficient TCV.

To fully appreciate DCL4 effects on TCV silencing, we used a recombinant virus (in vitro transcript inoculum of 500 ng/leaf) in which the *green fluorescent protein* (*gfp*) reporter-gene replaced the P38 sequence [TCV-GFPΔP38, Fig. 3A and (*16*)]. TCV-GFPΔP38 siRNAs accumulated as a 21-nt species in inoculated leaves of WT plants and single *dcl* mutants, except in *dcl4*, in which siRNAs were 22 nt long (Fig. 3A). Viral RNA levels were low in *dcl2* and *dcl3* mutants, but higher in *dcl4* and *dcl3-dcl4* plants (Fig. 3B), which suggested a greater antiviral contribution of DCL4 alone in TCV-GFPΔP38 than in TRV-PDS infections (Fig. 1D). TCV-GFPΔP38 levels were extremely high in *dcl2-dcl4* (Fig. 3B), consistent with results of *dcl2-dcl4* and *dcl2-dcl3-dcl4* mutants infected with wild-type TCV (Fig. 2B). Although 24-nt siRNAs were undetectable in WT-infected plants, they accumulated in *dcl2-dcl4* plants (Fig. 3C), as in TRV-PDS–infected plants (Fig. 1E). Also as with TRV-PDS, very low siRNA levels were detected in *dcl2-dcl3-dcl4*, likely reflecting inefficient DCL1 activities (Fig. 3C). We conclude that a similar DCL consortium affected siRNA production and virus levels in plants infected with TRV-PDS or TCV-GFPΔP38, and that DCL4 and DCL2 redundantly mediate defense against P38-deficient TCV.

The loss of DCL2 had only limited impact on TCV susceptibility (Fig. 2, A and B). Likewise, *CHS* silencing was released in P38-expressing and TCV-infected plants, despite accumulation of 22-nt siRNAs (Fig. 2C). This suggested that 22-nt siRNAs had suboptimal antiviral activity in the presence of P38. Accordingly, transgenic P38 prevented VIGS, promoted strong disease symptoms and high accumulation of TRV-PDS (Fig. 3D; fig. S2), effects that specifically required the combined inactivation of DCL2 and DCL4 in nontransgenic plants (Fig. 1, E and L). We conclude that besides primary DCL4-antagonizing activities, P38 also likely suppresses the action of DCL2-dependent siRNAs, consistent with major antiviral roles for both enzymes. Further demonstrating the key antiviral functions of DCL4 and DCL2, Cucumber mosaic virus (CMV) levels were three to four times those in *dcl2-*

dcl4 plants compared with WT or single *dcl2* or *dcl4* mutants. Unlike TCV and TRV, however, CMV silencing was dependent on RDR6 (*14*), loss of which resulted in CMV levels that were indistinguishable from those in *dcl2-dcl4* double mutants (fig. S3).

DCL2-DCL4–dependent block to systemic virus movement.

We exploited the GFP tag to follow TCV-GFPΔP38 infection in WT and *dcl* mutant plants, initially using a moderate in vitro transcript inoculum (500 ng/leaf). TCV-GFPΔP38 moved from cell to cell to form scattered primary lesions in WT-inoculated leaves (Fig. 4A, inlay) but consistently failed to spread systemically and produced no disease symptom (Fig. 4, B and C) (*16*). Those defects were rescued in P38 transgenic plants (Fig. 4, D to F), which exhibited large, confluent primary lesions in inoculated leaves (Fig. 4D). The aborted systemic spread of TCV-GFPΔP38 could have resulted from its failure to counteract the DCL4-DCL2 antiviral effects, owing to the lack of P38. However, because P38 is also the viral capsid, it could have simply resulted from an inability to form virions, a prerequisite to systemic infection of many plant viruses (*17*).

To address these issues, we used the *Arabidopsis* amplicon line (AMP, in SOM Text) in which replication of a GFP-tagged RNA virus triggers silencing of viral transcripts and low GFP accumulation (Fig. 4, G and H). Transgenic P38 (line AMP-P38) and TCV infection suppressed amplicon silencing [Fig. 4, G (middle and bottom), and H] and inhibited accumulation of endogenous ta-siRNA255 (Fig. 4H). A genetic screen for loss of the AMP-P38 phenotype identified two mutants, m1 and m2, that exhibited reduced amplicon RNA accumulation and GFP expression and also contained WT ta-siRNA255 levels (Fig. 4H). Linkage analysis, DNA sequencing and immunoblot assays revealed that m1 and m2 were stable, point-mutation alleles of P38 (Fig. 4, H and I). The data presented are for m1; similar results were obtained with m2.

Despite extensive cell-to-cell movement in inoculated leaves to levels resembling those of virion-proficient P38 plants (Fig. 4D), long-distance spread of TCV-GFPΔP38 was prevented in plants having m1 or m2 mutations in which the AMP locus had been segregated away (Fig. 4J, top). However, both P38 alleles formed virions, because TCV-GFPΔP38 was transmitted from infected plants with m1 or m2 mutations to healthy, P38-expressing plants through sap inoculation, a procedure whereby viral RNAs that are not encapsidated are rapidly degraded (Fig. 4J, bottom). Thus, m1 or m2 genetically uncoupled the virion-packaging and suppression of silencing functions of P38. Therefore, the lack of systemic TCV-GFPΔP38 P38 movement in WT plants was not caused by its inability to form virions, but rather, by its likely failure to counteract the DCL4-DCL2 antiviral effects. To test this idea, a moderate TCV-GFPΔP38 inoculum (500 ng/leaf) was applied to *dcl2, dcl4*, and *dcl2-dcl4* mutants. Whereas the infection phenotype of *dcl2* mutants was indistinguishable from that of WT plants, *dcl4* mutants exhibited large

primary lesions (Fig. 4K, left) but failed to support systemic movement (Fig. 4K, right). By contrast, there were confluent primary lesions, systemic movement, and disease symptoms in *dcl2-dcl4* plants (Fig. 4L). We conclude that, with a moderate inoculum, the combined loss of DCL4 and DCL2 functions was necessary and sufficient to recapitulate the P38-mediated rescue of P38-deficient virus infection.

DCL4 imposes a barrier to vascular exit of TCV-GFPΔP38.

The continuum of infection phenotypes in WT, *dcl4*, and *dcl2-dcl4* plants suggested that the primary effect of DCL2 and DCL4 was to restrict the virus to inoculated leaves (Fig. 4, A, K, and L). A fivefold increase in TCV-GFPΔP38 inoculum (5×, 2.5 μg/leaf) restored systemic movement in *dcl4*-, *dcl2-dcl4*–, and *dcl2-dcl3-dcl4*–inoculated plants, but in none of the other single or combination mutants (Fig. 5, A to C). Moreover, primary infection foci in *dcl4*-inoculated leaves were confluent, as in P38-expressing plants (Fig. 5C). By contrast, and despite formation of macroscopic primary foci, the same (2.5 μg/leaf, Fig. 4D) or much higher-dose (25×, 12.5 μg/leaf) inocula failed to promote systemic movement in WT plants, even though the virus consistently entered the petiole vasculature (Fig. 5, D and E, arrows). Therefore, increasing the inoculum strength could bypass the antiviral effects of DCL2 but not those of DCL4.

To gain insight into additional antiviral roles of DCL4, TCV-GFPΔP38–inoculated leaves were examined in greater detail. GFP was evenly distributed in petioles of *dcl4* plants (Fig. 5C, arrow), whereas in similar WT tissues it appeared as thin stripes (Fig. 5, D and E, arrows), identified as vascular bundles (Fig. 5, F to I). In contrast, TCV-GFPΔP38 could readily exit the vasculature of *dcl4* petioles, invading parenchyma and epidermal cells (Fig. 5, J and K). Thus, although the virus penetrated the phloem of WT plants, its unloading was specifically prevented by a DCL4-dependent mechanism. This mechanism was likely not cell autonomous, because it was also manifested in petioles of high-dose inoculated WT leaves (12.5 μg inoculum per leaf) in which virus accumulation was likely as elevated as in *dcl4* tissues (Fig. 5, E compared with C).

We recently identified DCL4 as an essential component of non–cell autonomous RNA silencing in a genetic screen using the *SUC-SUL* system, whereby a vascular-specific IR transgene triggers *SUL* silencing movement, resulting in vein-centered chlorosis [(7), Fig. 5L]. Of the two *SUC-SUL*–derived siRNAs species (21-nt and 24-nt; Fig. 5L), only DCL4-dependent 21-nt siRNAs were found required for cell-to-cell signaling (7). We reasoned that the vein-restriction of TCV-GFPΔP38 could have resulted from its failure to suppress the effects of an antiviral, DCL4-dependent silencing signal (Fig. 5Q). If so, P38 and TCV were expected to inhibit vascular exit of silencing signals. Transgenic P38 and TCV infection indeed alleviated silencing movement in *SUC-SUL* plants (Fig. 5, M to O). Moreover, the 21-nt siRNA levels were reduced in TCV-infected tissues (Fig. 5P), recapitulating the effects

of *dcl4* knockout mutations that specifically prevented *SUL* silencing movement (*7*). Collectively, these results support the ideas that DCL4 exerts some of its antiviral effects by producing a silencing signal that restricts virus exit from vascular bundles, and that vascular production of P38 inhibits this signaling during normal infections (Fig. 5Q).

Conclusions

Although virus-derived dsRNA is accessible to each of the four DCLs under appropriate genetic circumstances, DCL4 and DCL2 exhibit specific, hierarchical antiviral activities. The primary sensor is DCL4, which produces 21-nt siRNAs that guide a virus-antagonizing RISC. Secondarily, DCL2 forms 22-nt siRNAs with antiviral activities, but these are manifested prominently when DCL4 is genetically removed or suppressed. Hyper-susceptibility was only evident when both enzymes were inactivated, which revealed their combined action in defense. Despite detection of DCL3 and, to a limited extent, DCL1 activities on virus-derived substrates, these were not associated with antiviral defense. The hierarchical DCL access to virus-derived dsRNAs is similar to that detected with ta-siRNA precursors: Ta-siRNA biogenesis involves the preferential activity of DCL4, but both DCL3 and DCL2 gain access to precursors in *dcl4* mutants (*5*, *6*). Such specificity and hierarchical action possibly reflect contrasted DCL affinities for distinct dsRNA substrates and are likely to apply to viruses impacted by RDR6, such as CMV, and to viruses with DNA genomes (*18*).

Previous studies suggested that P38 suppresses one DCL (*15*), and we show that DCL4 is the primary target. However, DCL4 suppression was rescued by DCL2, although the antiviral activity of 22-nt siRNAs was in turn compromised by P38. Have DCL4 and DCL2 evolved primarily for optimal, redundant processing of various forms of pathogenic dsRNA? The existence of endogenous ta-siRNAs and nat-siRNAs that involve DCL4 and DCL2, respectively, complicates this question (*5*, *6*, *8*). However, exposure to highly diverse viral suppressors that impact DCL functions may explain why the DCL family has proliferated in plants and why DCL4 and DCL2 diverge in sequence much faster than the miRNA-specific DCL1 (SOM Text). Nevertheless, several silencing suppressors directly sequester DCL products, and these may differently influence evolution of silencing components (*19*).

Finally, this study indicates that a full appreciation of plant antiviral silencing will require analysis of viral genomes with disabled silencing suppressor functions. This notably uncovered the specific effects of DCL4 on virus vascular exit. The finding that TCV movement required the suppressor function of P38 independently of its virion-packaging function sheds a new light on systemic movement by offering a molecular explanation as to why the bundle sheath–phloem interface usually acts as a key boundary against long-distance transport of most plant viruses (*17*).

References and Notes

1. E. Bernstein, A. A. Caudy, S. M. Hammond, G. J. Hannon, *Nature409*, 363 (2001).
2. D. Baulcombe, *Nature431*, 356 (2004).
3. D. P. Bartel, *Cell116*, 281 (2004).
4. Z. Xie et al., *PLoS Biol.2*, E104 (2004).
5. V. Gasciolli, A. C. Mallory, D. P. Bartel, H. Vaucheret, *Curr. Biol.* (2005).
6. Z. Xie, E. Allen, A. Wilken, J. C. Carrington, *Proc. Natl. Acad. Sci. U.S.A.102*, 12984 (2005).
7. P. Dunoyer, C. Himber, O. Voinnet, *Nat. Genet.37*, 1356 (2005).
8. O. Borsani, J. Zhu, P. E. Verslues, R. Sunkar, J. K. Zhu, *Cell123*, 1279 (2005).
9. A. J. Hamilton, D. C. Baulcombe, *Science286*, 950 (1999).
10. O. Voinnet, *Nat. Rev. Genet.6*, 206 (2005).
11. X. H. Wang et al., *Science312*, 452 (2006).
12. P. Mourrain et al., *Cell101*, 533 (2000).
13. F. Schwach, F. E. Vaistij, L. Jones, D. C. Baulcombe, *Plant Physiol.138*, 1842 (2005).
14. F. Ratcliff, B. D. Harrison, D. C. Baulcombe, *Science276*, 1558 (1997).
15. F. Qu, T. Ren, T. J. Morris, *J. Virol.77*, 511 (2003).
16. Y. Cohen, A. Gisel, P. C. Zambryski, *Virology273*, 258 (2000).
17. H. B. Scholthof, *Trends Plant Sci.10*, 376 (2005).
18. R. Akbergenov et al., *Nucleic Acids Res.34*, 462 (2006).
19. L. Lakatos et al., *EMBO J.25*, 2768 (2006).

We thank members of the Voinnet laboratory for discussions and Z. Xie for *dcl* seeds. Funded by CNRS grant to A.D.; NSF grant MCB-0209836, NIH grant AI43288, and U.S. Department of Agriculture grant NRI 2005-35319-15280 to J.C.; and Pao Schloarship (Zhejiang University, China) to J.B. This work is dedicated to the memory of M. and G. Voinnet.

Supporting Online Material (SOM)

Material and Methods

Plant material

All mutant combinations were based on dcl1-9, dcl2-1, dcl3-1, dcl4-2, rdr1-1, rdr2, and rdr6-15, which were described previously (S1–S4). The dcl2-dcl3 and dcl2-dcl4 double mutant lines were as described (S3).The dcl3-dcl4 and dcl2-dcl3-dcl4 mutant lines were generated by standard genetic crosses. Homozygous mutant genotypes were confirmed by allele-specific PCR assays

after two generations. The Arabidopsis CHS RNAi, SUC-SUL and AMP transgenic lines were as described (S5–S7). The pBIN61-P38 construct (S8) was used for plant transformation with the Agrobacterium strain GV3101 according to (S9). Selection of transgenic plants was on medium containing 50 mg/ml kanamycin. All plants were grown in standard greenhouse conditions for 3 weeks, then in short-days conditions for 2-3 weeks before infection assays.

Mutagenesis and genetic screen for loss of P38 function in the AMP line

Seeds of the homozygous double-transgenic line P38 AMP (n = 10,000) were incubated for 16 h at room temperature in 10 mL of water containing 0.4% Ethyl-Methyl-Sulfonate (Sigma). EMS was then neutralized, seeds washed several times with water and planted in soil to allow selffertilization. Seeds produced were collected in bulks of 200 plants and sown on plates (MS medium) with appropriate selection. Seedlings were screened under UV for altered patterns of GFP-silencing suppression mediated by P38. The m1 and m2 mutants were identified visually and the integrity of the P38 protein assayed by Western analysis, using a P38 antibody (kindly provided Ann Simon, University of Maryland). The P38 gene was PCR-amplified from extracted genomic DNA, using primers specific for the 35S promoter and terminator of pBIN61 (S8) and it was subsequently sequenced (ABI prism capillary sequencing). The m1 mutation was found to be a GÆA transition replacing the glutamate residue at postion 121 for a lysine. The m2 mutation was a CÆT transition replacing the arginin residue at position 73 for a tryptophan. Note that both lesions are typically induced by EMS, used for mutagenesis.

The m1 and m2 locus were then segregated away from the AMP locus by crossing to WT plants (ecotype La-er) and allowing the progeny to self. F2 plants containing the P38 mutant alleles were selected on medium containing 50 mg/ml kanamycin and those showing weak GFP fluorescence (indicating the presence of the AMP locus) were discarded. The remaining plants were allowed to self to obtain both stable P38 mutant alleles in WT background. The same procedure was followed to segregate the WT P38 away from the AMP locus and to produce control plants that contain neither the AMP nor the P38 loci, used in the infections with TCVGFPΔP38.

Viruses and infection assays

The infectious clone of TRV-PDS, amplification of viral transcripts and inoculation of Arabidopsis plants were described before (S2). Infected/photobleached systemic leaves were collected at 14 dpi. The infectious clone of TCV and prior inoculation to Nicotiana benthamiana leaves by agro-infiltration were described before (S8); sap was subsequently extracted from those

leaves at 5 dpi (1 g tissue/2 mL 5 mM NaP pH 7.5) and used to inoculate Arabidopsis rosettes (about 5 to 6 weeks old, prior to bolting). Infected systemic leaves were collected at 14 dpi and subjected to molecular analyses (Northern blots, Western blots). Time-course analyses of TCV and CMV accumulation were based on total RNA from five (CMV) or six (TCV) individually inoculated or mock-inoculated plants. RNA was isolated by Trizol (Invitrogen) extraction from infected tissue and analyzed at multiple time points postinoculation. Analysis of TCV accumulation was carried out on plants inoculated with in-vitro transcripts as previously described (S1). Systemically-infected tissue was collected at 3, 7, 11 and 15 dpi. TCV genomic RNA was measured by densitometry from ethidium bromide-stained gels (AlphaImager, Alpha Innotech) and were standardized using the 26S ribosomal RNA, normalized to Col-O. Note that reduced accumulation of TCV-derived 22-nt siRNAs is observed at 7 dpi in dcl2 mutants inoculated with TCV viral transcripts at (S1) while this is observed at 14 dpi with sapinoculation, which delays the infection in comparison to the first method. Infections with CMV were described previously (S1). CMV genomic RNA was analyzed by northern blot and quantified by electronic autoradiography (InstantImager, Packard). The infectious clone of TCVGFPΔCP and in-vitro transcripts preparation were described before (S10). 500 ng or 2.5 µg of viral RNA transcripts per leaf were mixed 1:1 (v/v) with inoculation solution (200 mM K2HPO4, macaloid, yeast tRNA 0.4 µg/µl) to obtain a moderate and strong inoculum respectively, and gently rubbed with celite on four leaves of Arabidopsis rosettes. Plants were monitored daily for GFP activity from 5 dpi. Inoculated and systemic leaves were harvested at 7 dpi and 12 dpi respectively. P38 transgenic plants were used for sap-inoculation assays, in order to amplify viral transmission, when it occurred, and thereby make it appreciable visually.

Analysis of nucleic acids

RNA extraction procedures employed in TCV and CMV time course analyses are described in the previous section. Total RNA from leaves was extracted using Tri-Reagent (Sigma) according to the manufacturer's instructions, precipitated with isopropanol,and redissolved in 50% formamide. Northern analyses of low and high molecular weight RNA were performed with 15 µg and 5 µg of total RNA respectively, as described previously (S11). For small RNA analyses of TCV-GFPΔCP infected plants (Fig.2F), 30 µg were used. Ethidium bromide staining of total RNA before transfer was used to confirm equal loading. Radiolabeled probes for detection of PDS, RNA2, CHS, GFP and SUL RNAs were made by random priming reactions (Promega) in the presence of [α32P]dCTP. DNA fragments specific for the CHS, GFP and SUC transcripts were 256-, 800-, and 400-bp fragments respectively, PCR-amplified from Arabidopsis genomic DNA (S5, S6) or from the mGFP5 ORF (S12). The probe for the viral PDS insert was a 600-bp fragment amplified from Arabidopsis genomic DNA, as described (S6). Probes specific for the

PDS host RNA (upstream and downstream of the region corresponding to the viral insert) were 564- and 510-bp fragments respectively, amplified from Arabidopsis genomic DNA. The probe specific for TRV RNA2 was a 4-kb fragment excised by restriction digestion from plasmid TRV RNA2-GFP (S13).The probe specific for TCV RNA was a mix of two DNA oligonucleotides corresponding to TCV sequence that were end-labelled with [γ32P]ATP using T4 polynucleotide kinase (New England Biolabs). The same procedure was employed to detect trans-acting siRNAs 255, using an oligonulcleotide with complementary sequence. All primers and oligonucleotide sequences are available upon request.

Western blot analysis

Total proteins from P38-transgenic plants and TCV-infected plants, respectively were extracted in Laemmli buffer, resolved by SDSPAGE and transferred by electroblotting onto a polyvinylidene difluoride membrane (Immobilon-P; Millipore). TCV-P38 antiserum from rabbit (a kind gift of Ann Simon) was used at a dilution of 1/15000 and revealed by a second, peroxidase-conjugated antibody (Biosys) through enhanced chemiluminescence (Roche Lumilight PLUS).

GFP imaging

Pictures were taken under a Nikon SMZ15000 dissecting microscope coupled to a 100 W epifluorescence module. For transversal sections, plant material was embedded in 1% lowmelting-point agarose and cut either transversally or longitudinally.

SOM Text

1. The Arabidopsis Amplicon (AMP) silencing system is based on a transgene that encodes replication-competent Potato virus X (PVX, RNA virus) with a GFP insert (S14). Although Arabidopis is not a natural host for PVX, the virus can replicate at a low level. dsRNA derived from virus replication triggers RNA silencing directed against the viral transcripts and against primary, non-replicative trangene transcripts. This results in a self-sustaining loop whereby PVXGFP levels (and, consequently, GFP accumulation) are maintained at a very low level. Consequently, AMP plants appear red, owing to chlorophyll fluorescence under UV.

2. Analysis of individual Arabidopsis DCL and their orthologous counterparts in medicago, rice, maize, and poplar indicates that DCL1 is under much more negative selection than are DCL3 and DCL2 (O. Voinnet and J. C. Carrington)

SOM References

S1. Z. Xie et al., PLoS Biol 2, E104 (May, 2004).
S2. D. Yu, B. Fan, S. A. MacFarlane, Z. Chen, Mol Plant Microbe Interact 16, 206 (2003).
S3. Z. Xie, E. Allen, A. Wilken, J. C. Carrington, Proc Natl Acad Sci U S A 102, 12984 (2005).
S4. E. Allen, Z. Xie, A. M. Gustafson, J. C. Carrington, Cell 121, 207 (Apr 22, 2005).
S5. P. Dunoyer, C. H. Lecellier, E. A. Parizotto, C. Himber, O. Voinnet, Plant Cell 16, 1235 (2004).
S6. P. Dunoyer, C. Himber, O. Voinnet, Nat Genet 37, 1356 (2005).
S7. T. Dalmay, A. J. Hamilton, E. Mueller, D. C. Baulcombe, Plant Cell 12, 369 (2000).
S8. C. L. Thomas, V. Leh, C. Lederer, A. J. Maule, Virology 306, 33 (2003).
S9. N. Bechtold, G. Pelletier, Methods Mol Biol 82, 259 (1998).
S10. Y. Cohen, A. Gisel, P.C. Zambryski, Virology 273, 258 (2000).
S11. C. Himber, P. Dunoyer, G. Moissiard, C. Ritzenthaler, O. Voinnet, EMBO J 22, 4523 (2003).
S12. O. Voinnet, P. Vain, S. Angell, D. C. Baulcombe, Cell 95, 177 (1998).
S13. S. A. MacFarlane, A. H. Popovich, Virology 267, 29 (2000).
S14. T. Dalmay, A. J. Hamilton, E. Mueller, D. C. Baulcombe, Plant Cell 12, 369 (2000).

Figure legends

Fig. 1. (A) Genome organization of TRV and its TRV-PDS derivative. (B and C) Asymptomatic infection (B) and extensive photobleaching (C) caused by TRV and TRV-PDS, respectively. (D and E) Analysis of (top) low- and (bottom) high-molecular-weight RNAs from TRV-PDS–infected plants carrying single (D) and double (E) *dcl* mutations [14 days post inoculation (dpi)]. The probe was specific for viral PDS. The numbers of infected plants showing photobleaching are from four independent experiments involving four plants each. (F to L) Disease symptoms and VIGS in *dcl* mutants (14 dpi). (M) TRV-PDS siRNA analysis in *dcl2-dcl3-dcl4* triple mutants (14 dpi). rRNA shown by ethidium bromide staining.

Fig. 2. (A) TCV genome organization; TCV siRNA (top) and coat-protein (P38) accumulations (bottom) in single or double *dcl* mutants (14 dpi). Prot, total protein staining. (B) Time-course analysis of TCV genomic RNA accumulation. Variance analysis of the data from 15 dpi produced five statistical groups (a to e). (C) Analysis of high (top) and low (second from top) molecular-weight RNAs derived from the inverted-repeat (IR) *CHS* locus in nontransgenic (NT), P38-transgenic (left) or TCV-infected plants (right). (Bottom) Accumulation of TAS255.

Fig. 3. (A) Genome organization of TCV-GFPΔP38 and TCV-GFPΔP38 siRNA analysis in *dcl* mutants (in vitro transcripts; 500 ng/leaf; 7 dpi). (B) TCV-GFPΔP38 RNA accumulation in single and double *dcl* mutants. The probe was GFP-specific. (C) TCV-GFPΔP38 siRNA analysis in double and triple *dcl* mutants and P38-expressing plants. (D) TRV-PDS–induced photobleaching occurs in WT, but not P38-expressing plants (14 dpi). (Right) TRV-PDS RNA accumulation. The numbers of infected plants showing photobleaching are from four independent experiments involving three plants each.

Fig. 4. (A) WT *Arabidopsis* leaf challenged with moderate TCV-GFPΔP38 inoculum (in vitro transcripts, 500 ng/leaf; 7 dpi). Chlorophyll fluoresces red under UV. (Inlay) Microscopic primary lesion. (B and C) Lack of symptoms (B) and of systemic virus movement (C) in the plant in (A). The numbers of infected plants showing systemic viral GFP are from three independent experiments involving five plants each. (D to F) Same as (A to C), but in P38-expressing plants. (G) GFP silencing in the amplicon (AMP, top) is released by transgenic P38 (AMP-P38) and TCV infection (middle and bottom). (H) Analysis of high- and low-molecular-weight RNAs from nontransgenic (NT), AMP, and AMP-P38 and from m1 and m2 mutants recovered after AMP-P38 mutagenesis. (Bottom) P38 immunoblot analysis. (I) Amino acid substitutions in m1 and m2 alleles of P38. (J) Confluent primary lesions and lack of systemic viral movement in m1 after high-dose inoculation (2.5 µg/leaf; top). TCV-GFPΔP38 is 100% transmitted from m1 to P38-expressing plants through sap extracts (bottom). (K) Same as (A to C) but in *dcl4* mutants. (L) Same as (A to C) but in *dcl2-dcl4* (14 dpi).

Fig. 5. (A) Systemic (syst) TCV-GFPΔP38 movement in *dcl4* plants challenged with high-dose inoculum (5×, 2.5 µg/leaf; inoc). (B) TCV-GFPΔP38 unloading in systemic *dcl4* leaves. (C) Confluent primary lesions and uniform GFP distribution (arrow) in petioles of *dcl4*-inoculated leaves. (D) Same as (C) but in WT plants. (E) The TCV-GFPΔP38 inoculum was five times that shown in (A) (25×, 12.5 µg/leaf). (F) Magnified view of the petiole in (E). Vasc, vascular bundles. (G and H) Transverse sections of (F). (I) Longitudinal section of (G) showing GFP confined into phloem cells. (J) Same as (F) but in *dcl4*-inoculated leaves. (K) Transverse section of (J). (L) The inverted-repeat (IR) *SUC-SUL* system. SUC2, phloem-specific promoter. (M) Transgenic P38 expression inhibits *SUL* silencing movement. (N) Loss of silencing movement in young tissues of TCV-infected *SUC-SUL* plants. (O) Magnified view of the apex in (N). Arrow, typical sink- (bottom leaf part, containing TCV) to-source (upper leaf part, not containing TCV) transition, showing that suppression of silencing movement is contingent on viral invasion. (P) *SUL* siRNA analysis in tissues depicted in (O). (Q) Model for dcl4-dependent vascular restriction of TCV-GFPΔP38 and its suppression by P38.

Fig. S1. (A-C). VIGS phenotypes of rdr1, rdr2 and rdr6 plants infected with TRV-PDS. (D)

Northern analysis of low (upper panel) and high (lower panel) molecular weight RNA extracted at 14 dpi from the plants depicted in (A-C) and from wild-type (WT) infected plants. rRNA: ethidium bromide staining of ribosomal RNA showing equal loading.(E) The RNA blot in Figure 1D was stripped and re-probed with a TRV-RNA2-specific probe (upper panel) or with a probe corresponding to the part of the PDS gene that did not overlap with the viral PDS insert. The results presented here are from a region located 5' of the viral insert, but identical results were obtained with a probe from the 3' region. (F) Analysis of high-molecular weight RNA and VIGS phenotype in triple dcl2-dcl3-dcl4 mutants infected with TRV-PDS (14 dpi). The values at the bottom are from 4 independent experiments involving 4 plants each except for dcl2-dcl3-dcl4 for which experiments involved 3 plants each. The values indicate the number of infected plants showing photo-bleaching. (G) Severe disease symptoms in the dcl2-dcl3-dcl4 triple mutants. Limited and sporadic photo-bleaching was occasionally observed (4 out of 12 plants tested), as indicated by the arrows. rRNA: ethidium bromide staining of ribosomal RNA showing equal loading.

Fig. S2. (A) Northern analysis of low molecular weight RNA extracted at 14 dpi from rdr1, rdr2 and rdr6 plants infected with TCV. rRNA: ethidium bromide staining of ribosomal RNA showing equal loading.(B-D) Disease symptoms developing on TCV-infected dcl2-dc3, dcl2-dcl4 and dcl4 mutant plants are indistinguishable. The pictures were taken at 14 dpi. (E) Analysis of TRV-PDS-derived siRNAs accumulating on WT plants or on P38 transgenic plants (as depicted in Fig.3D). Due to high siRNA accumulation preventing accurate size resolution (as a result of P38-mediated silencing suppression), the original P38 sample (1:1) was diluted 5 times in water (1:5). A 21-nt→22-nt shift is clearly seen in the track with the diluted sample, indicating that P38 suppresses DCL4 during TRV infections.

Fig. S3. Genome organization of Cucumber mosaic virus (CMV) and time course analysis of virus accumulation, assayed by Northern analysis, in the various dcl mutants and combinations thereof. The mean relative accumulation (±SD) is plotted for each mutant. Analysis of variance of the 21 dpi data, using the ANOVA Duncan's multiple range test ($p < 0.05$), produced two statistical groups (a, b). Note that CMV, unlike TRV and TCV, is clearly impacted by RDR6. Note also that the effects of dcl2-dcl4 double mutations are statistically equivalent to those of rdr6 knockouts. These results strongly suggest that DCL2 and DCL4 cooperate in a single pathway with RDR6 and, therefore, are also major antiviral determinants in plant-virus interactions involving host-directed siRNA amplification mechanisms.

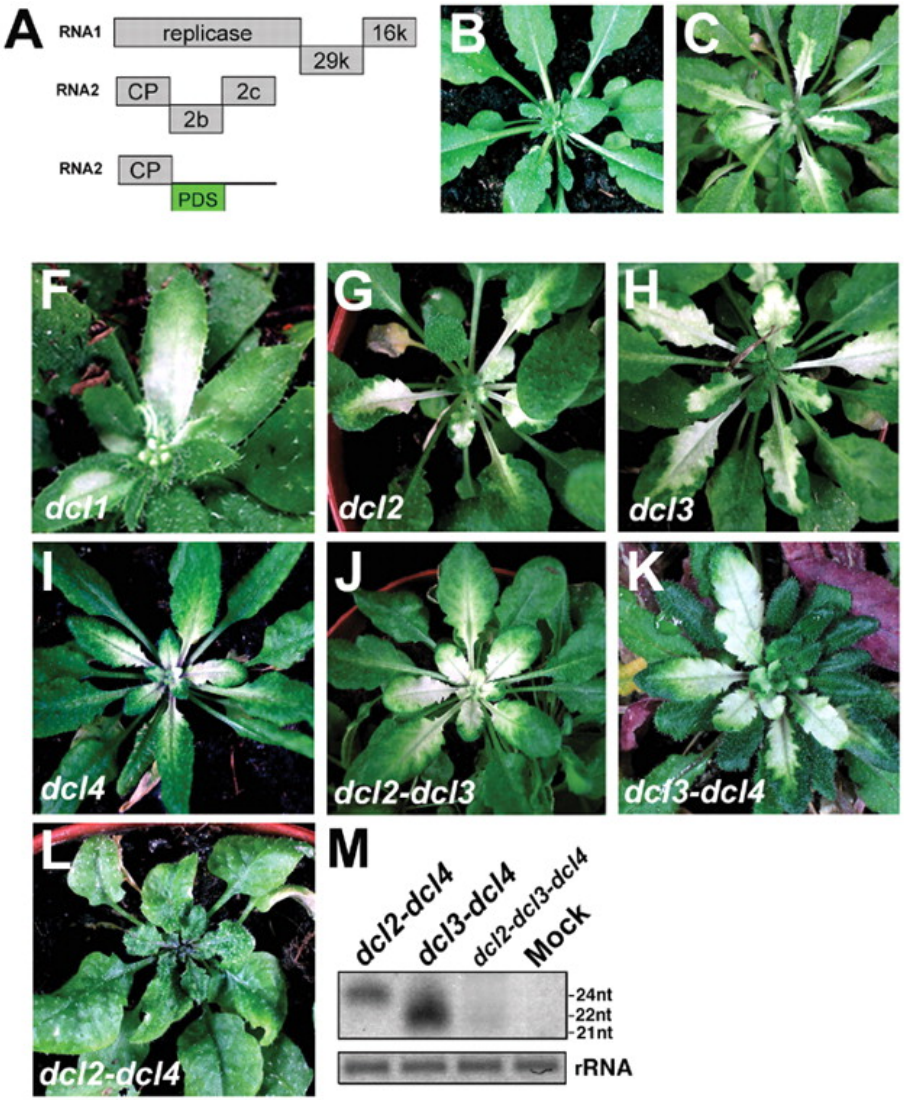
A
RNA1
replicase
16k
29k
RNA2
CP
2c
2b
RNA2
CP
PDS
B
C
F
dcl1
G
dcl2
H
dcl3
I
dcl4
J
dcl2-dcl3
K
dcl3-dcl4
L
dcl2-dcl4
M
dcl2-dcl4
dcl3-dcl4
dcl2-dcl3-dcl4
Mock
24nt
22nt
21nt
rRNA

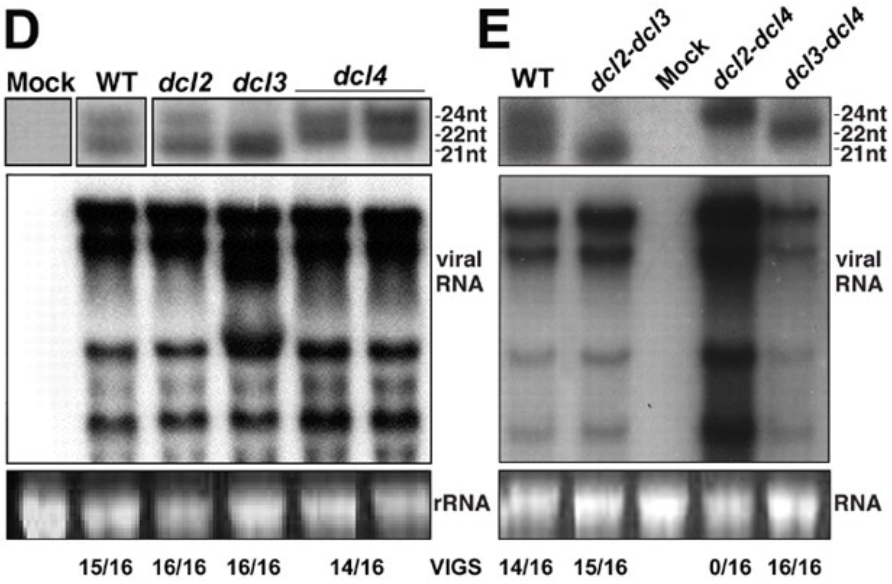
D
Mock
WT
dcl2
dcl3
dcl4
24nt
22nt
21nt
viral RNA
rRNA
15/16
16/16
16/16
14/16
VIGS
E
WT
dcl2-dcl3
Mock
dcl2-dcl4
dcl3-dcl4
24nt
22nt
21nt
viral RNA
RNA
14/16
15/16
0/16
16/16

Fig1

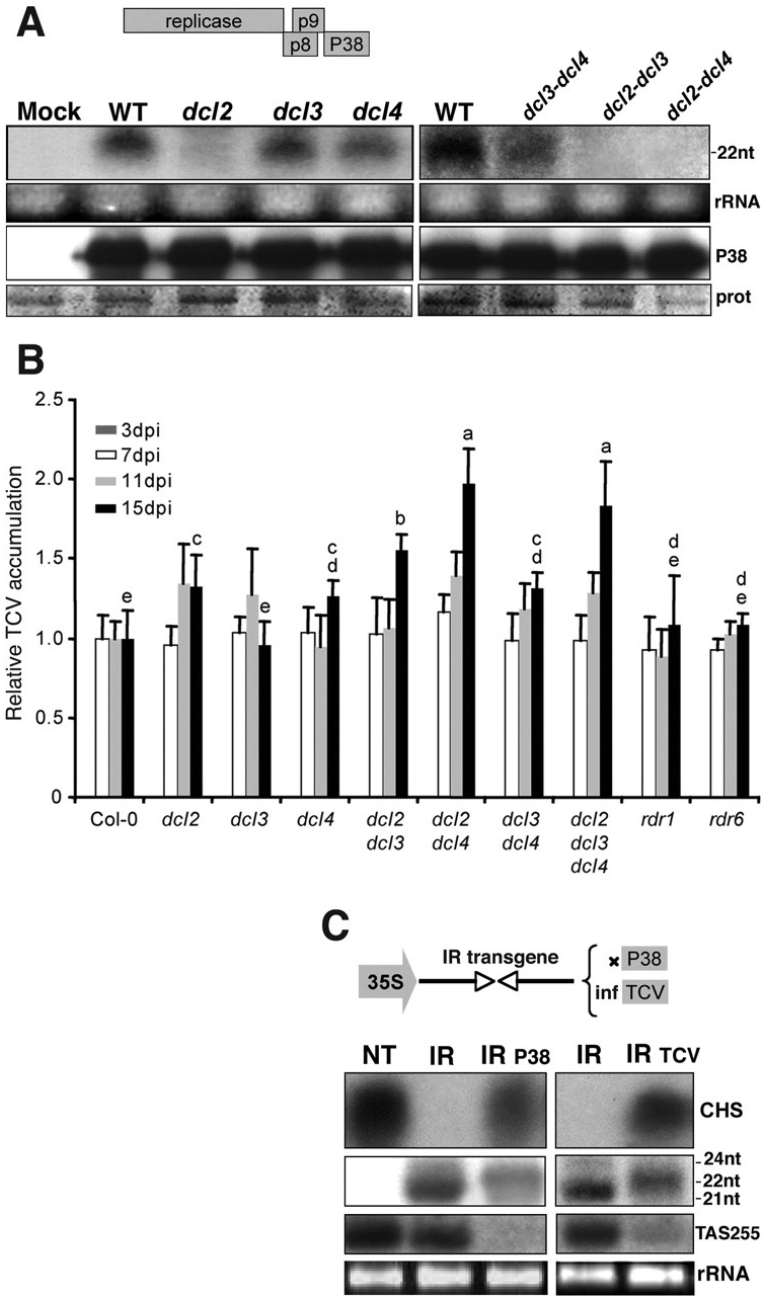
A
replicase
p9
p8
P38
Mock
WT
dcl2
dcl3
dcl4
WT
dcl3-dcl4
dcl2-dcl3
dcl2-dcl4
22nt
rRNA
P38
prot
B
Relative TCV accumulation
3dpi
7dpi
11dpi
15dpi
Col-0
dcl2
dcl3
dcl4
dcl2 dcl3
dcl2 dcl4
dcl3 dcl4
dcl2 dcl3 dcl4
rdr1
rdr6
C
35S
IR transgene
P38
TCV
NT
IR
IR P38
IR
IR TCV
CHS
24nt
22nt
21nt
TAS255
rRNA

Fig2

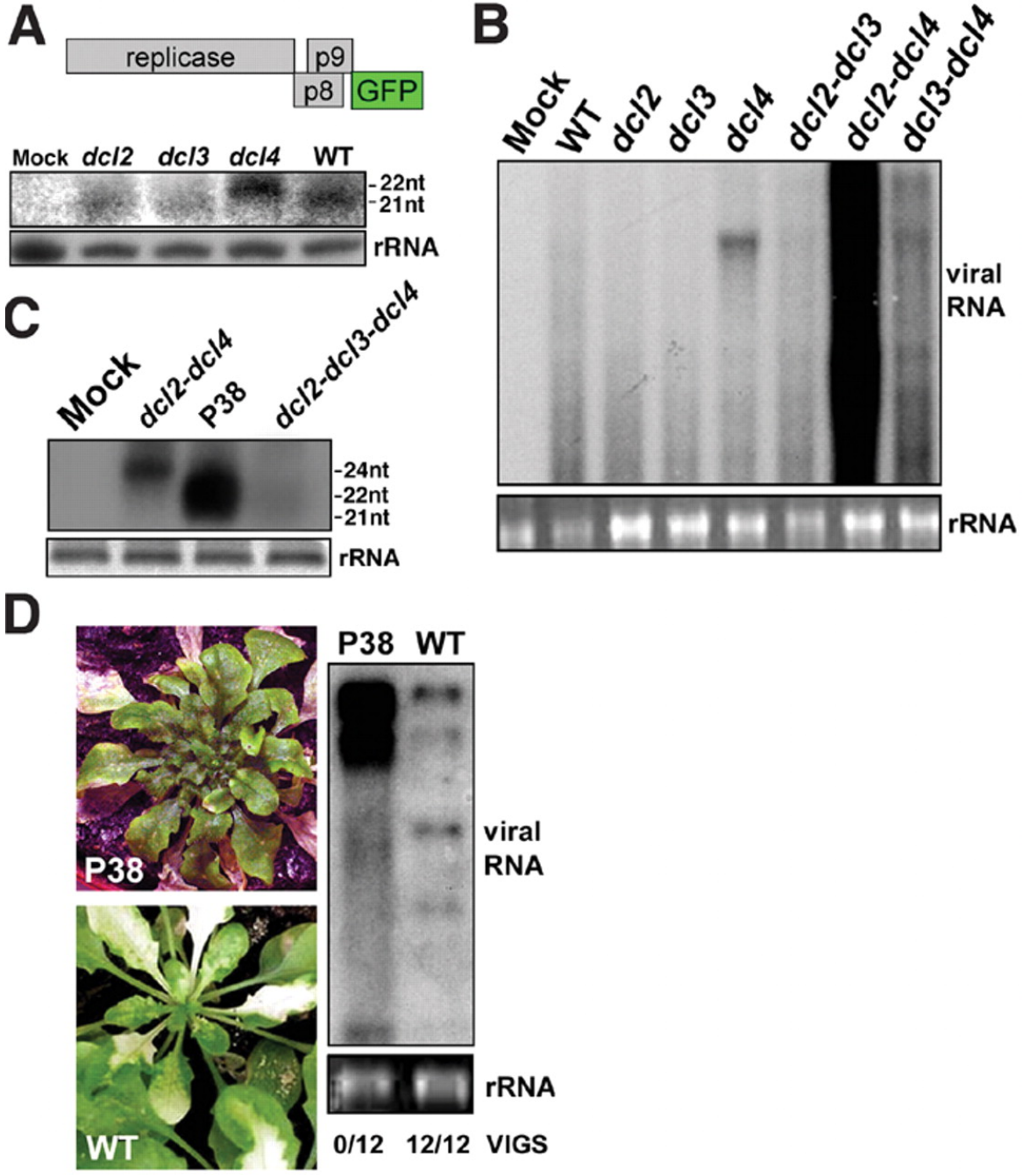
A
replicase
p9
p8
GFP
Mock
dcl2
dcl3
dcl4
WT
22nt
21nt
rRNA
B
Mock
WT
dcl2
dcl3
dcl4
dcl2-dcl3
dcl2-dcl4
dcl3-dcl4
viral RNA
rRNA
C
Mock
dcl2-dcl4
P38
dcl2-dcl3-dcl4
24nt
22nt
21nt
rRNA
D
P38
WT
viral RNA
rRNA
0/12
12/12
VIGS

Fig3

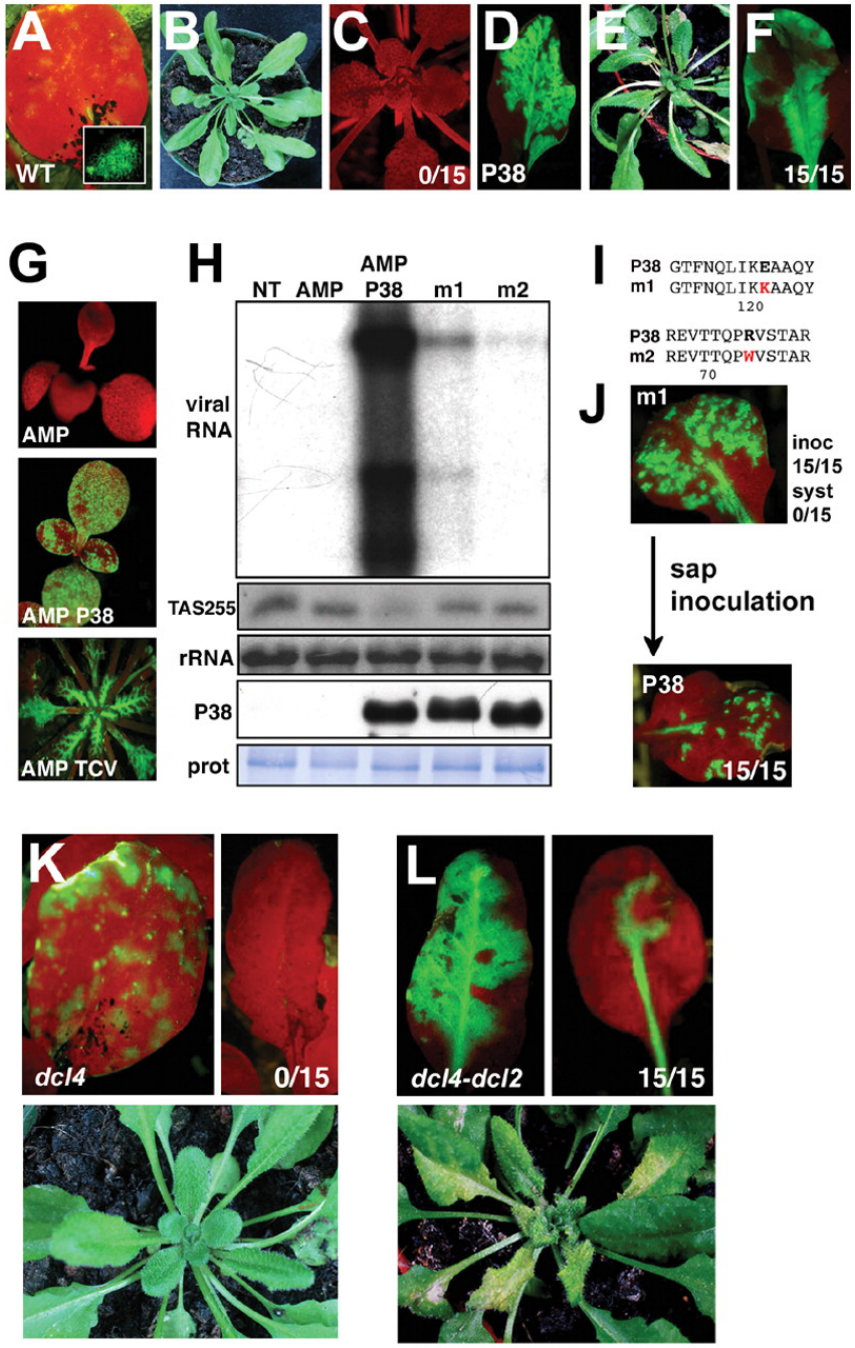
A
WT
B
C
0/15
D
P38
E
F
15/15
G
AMP
AMP P38
AMP TCV
H
AMP
NT AMP P38 m1 m2
viral RNA
TAS255
rRNA
P38
prot
I
P38 GTFNQLIKEAAQY
m1 GTFNQLIKKAAQY
120
P38 REVTTQPRVSTAR
m2 REVTTQPWVSTAR
70
J
m1
inoc 15/15
syst 0/15
sap inoculation
P38
15/15
K
dcl4
0/15
L
dcl4-dcl2
15/15

Fig4

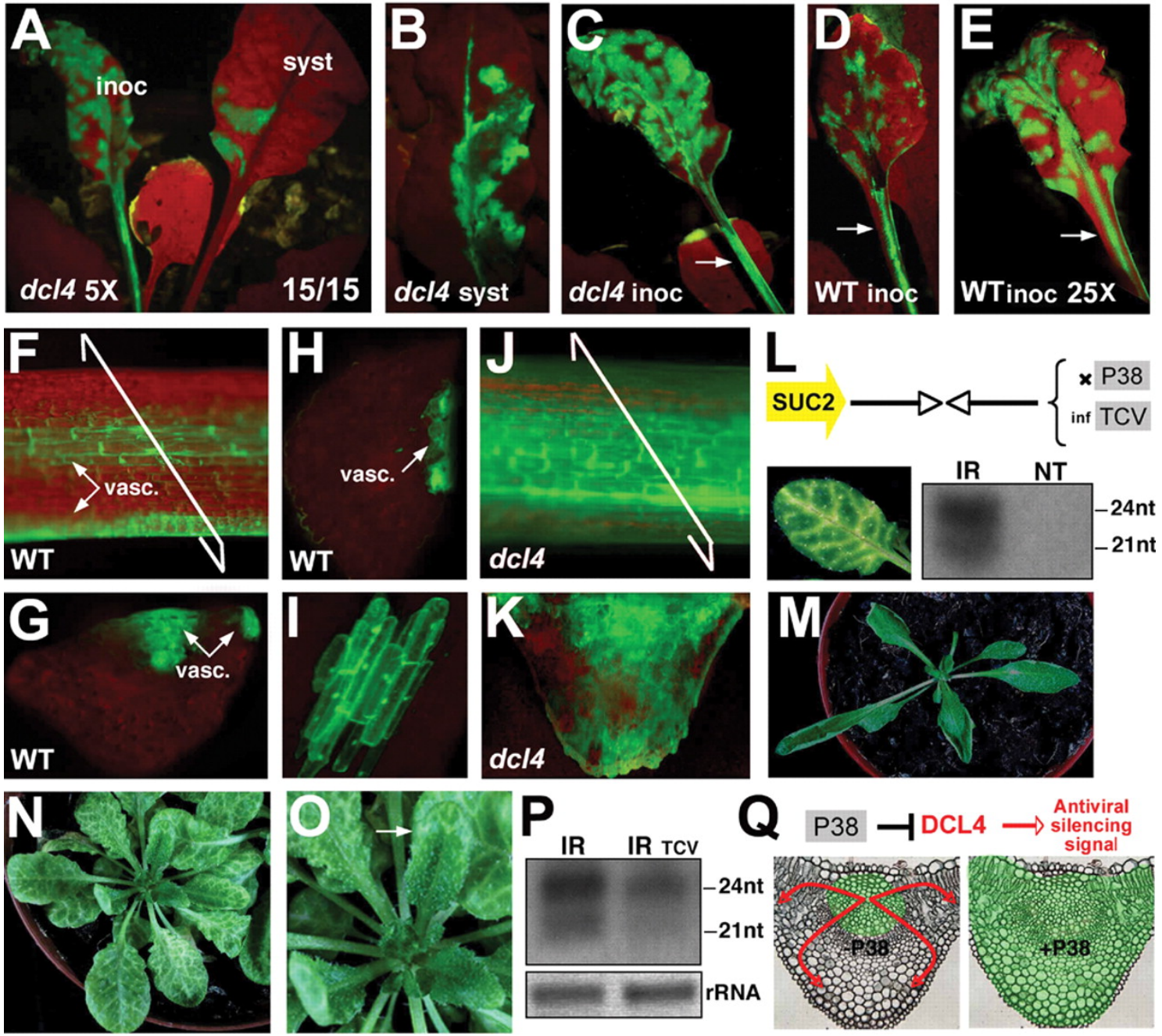
A
inoc
syst
dcl4 5X
15/15
B
dcl4 syst
C
dcl4 inoc
D
WT inoc
E
WTinoc 25X
F
vasc.
WT
H
vasc.
WT
J
dcl4
L
SUC2
P38
inf TCV
IR
NT
24nt
21nt
G
vasc.
WT
I
K
dcl4
M
N
O
P
IR
IR TCV
24nt
21nt
rRNA
Q
P38
DCL4
Antiviral silencing signal
P38
+P38

Fig5

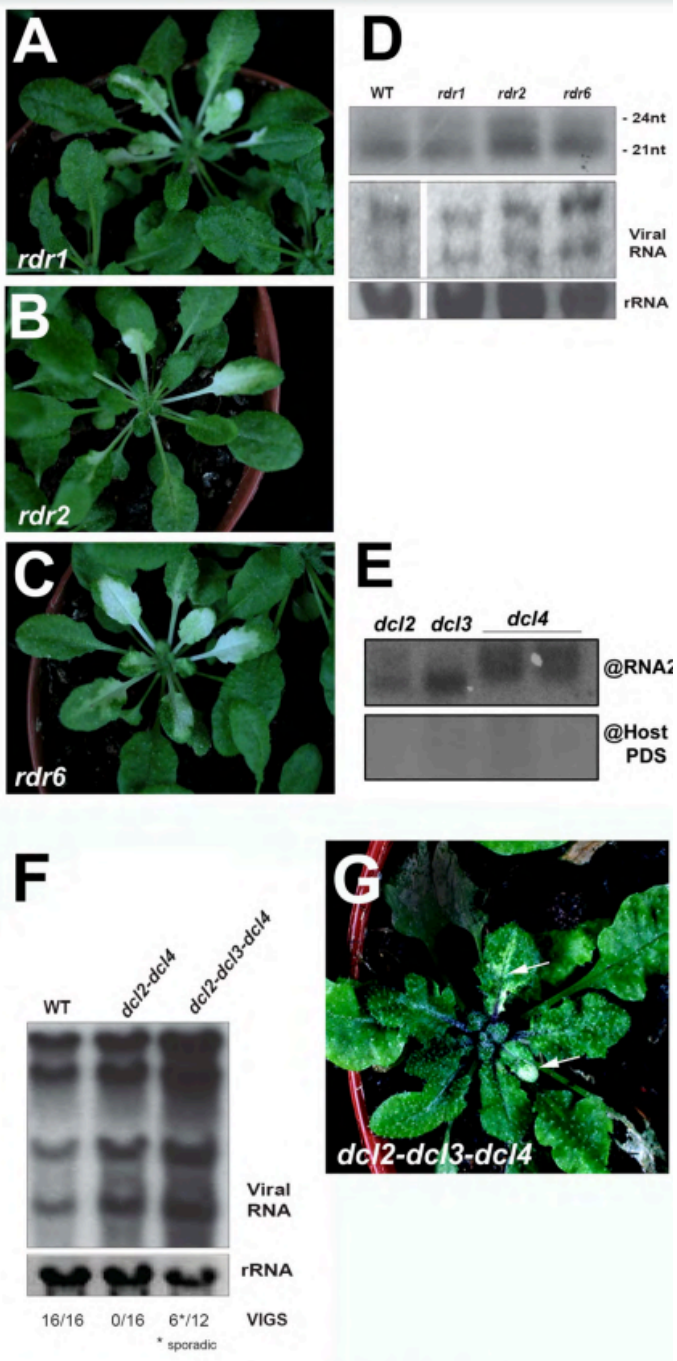
A
rdr1
B
rdr2
C
rdr6
D
WT
rdr1
rdr2
rdr6
- 24nt
- 21nt
Viral RNA
rRNA
E
dcl2
dcl3
dcl4
@RNA2
@Host PDS
F
WT
dcl2-dcl4
dcl2-dcl3-dcl4
Viral RNA
rRNA
16/16
0/16
6*/12
VIGS
* sporadic
G
dcl2-dcl3-dcl4

FigS1

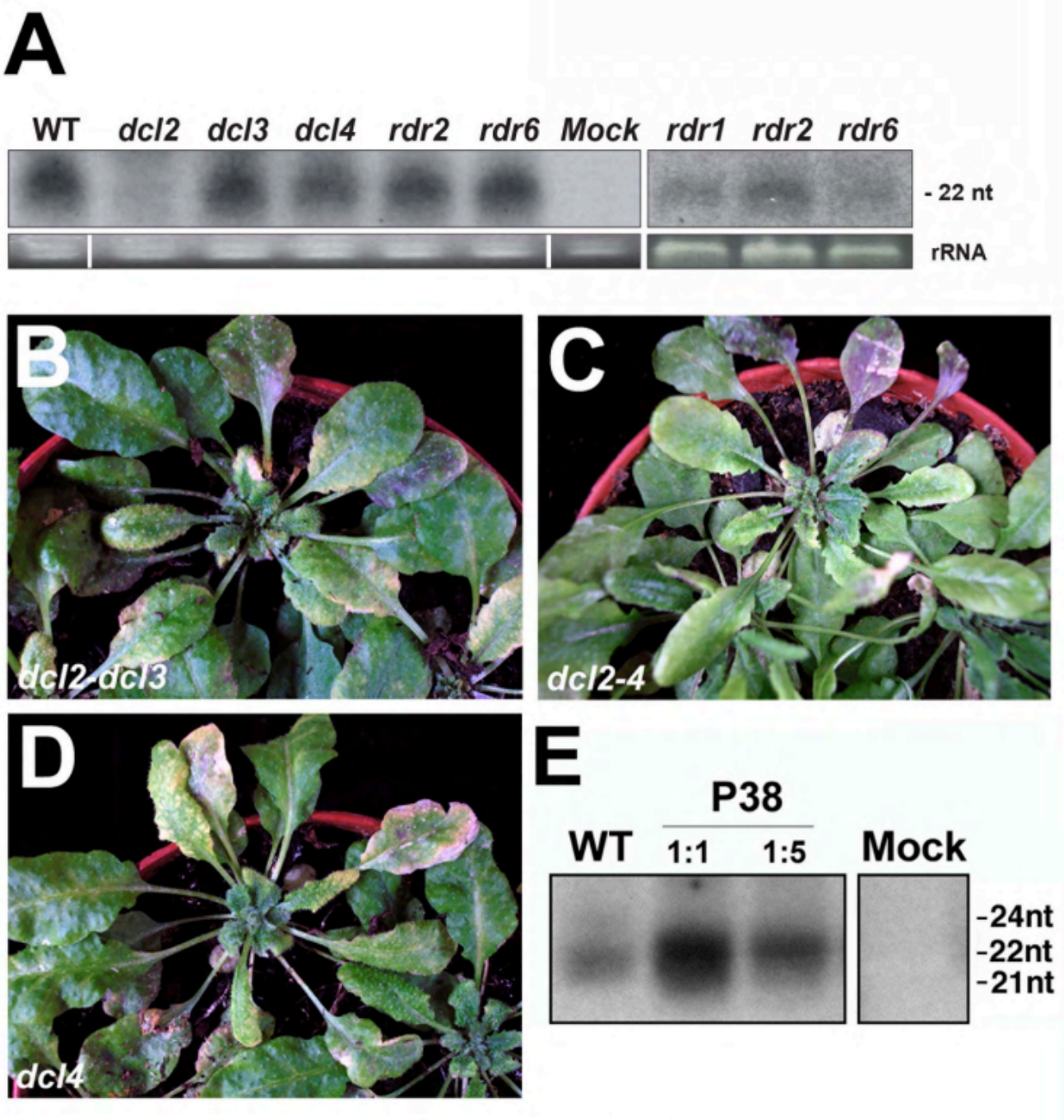
A
WT
dcl2
dcl3
dcl4
rdr2
rdr6
Mock
rdr1
rdr2
rdr6
- 22 nt
rRNA
B
dcl2-dcl3
C
dcl2-4
D
dcl4
E
P38
WT
1:1
1:5
Mock
-24nt
-22nt
-21nt

FigS2

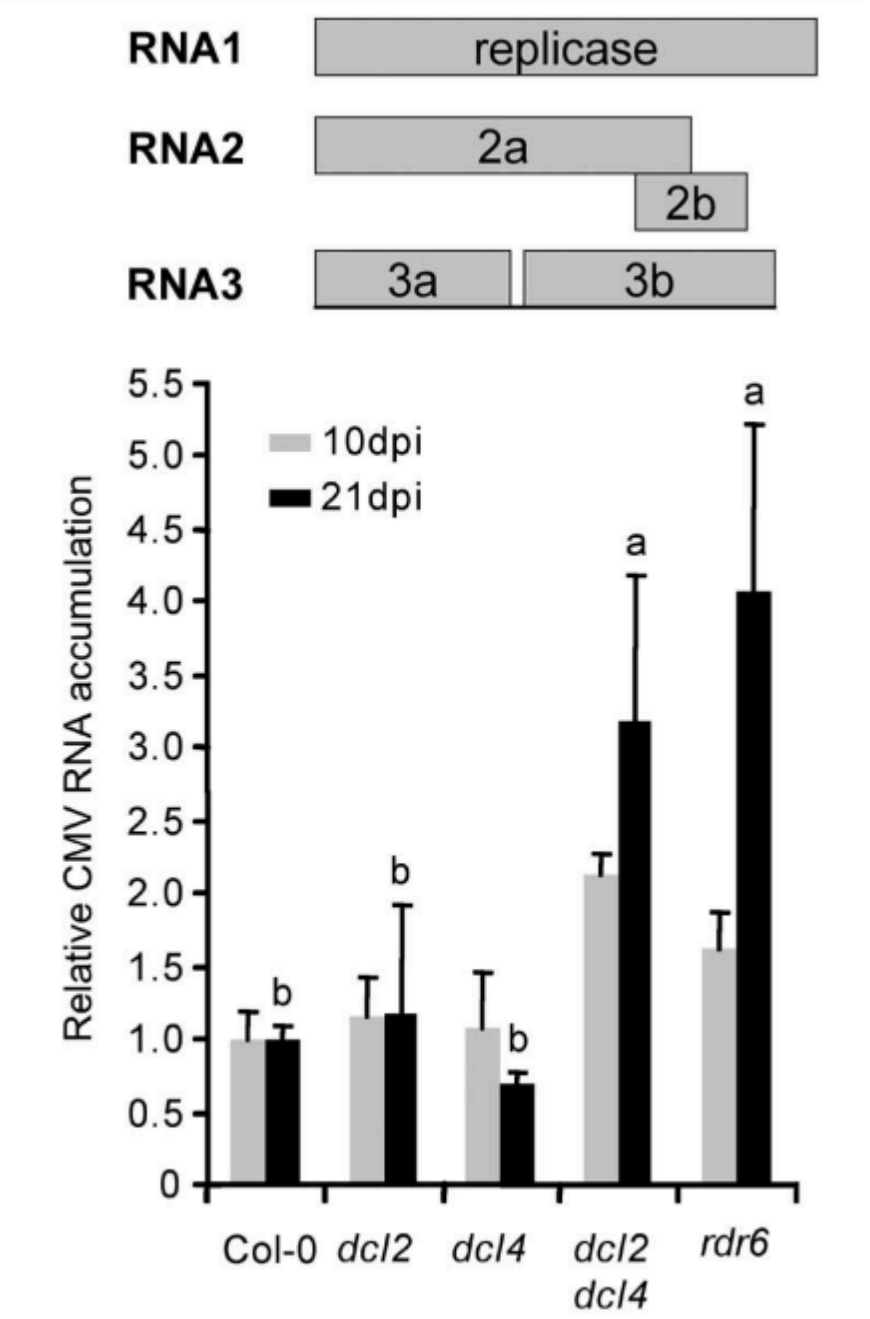
RNA1
replicase
RNA2
2a
2b
RNA3
3a
3b
Relative CMV RNA accumulation
10dpi
21dpi
5.5
5.0
4.5
4.0
3.5
3.0
2.5
2.0
1.5
1.0
0.5
0
a
a
b
b
b
Col-0
dcl2
dcl4
dcl2 dcl4
rdr6

FigS3